



HAL
open science

Atomic-Spring-like Effect in Glassy Silica-Helium Composites

Daniel T Bowron, David A Keen, Mathieu Kint, Coralie Weigel, Benoit Ruffle, Leszek Konczewicz, Sylvie Contreras, Benoit Coasne, Gaston Garbarino, Mickael Beaudhuin, et al.

► **To cite this version:**

Daniel T Bowron, David A Keen, Mathieu Kint, Coralie Weigel, Benoit Ruffle, et al.. Atomic-Spring-like Effect in Glassy Silica-Helium Composites. *Journal of Physical Chemistry C*, 2022, 126 (12), pp.5722-5727. 10.1021/acs.jpcc.2c00026 . hal-03821835

HAL Id: hal-03821835

<https://cnrs.hal.science/hal-03821835>

Submitted on 19 Oct 2022

HAL is a multi-disciplinary open access archive for the deposit and dissemination of scientific research documents, whether they are published or not. The documents may come from teaching and research institutions in France or abroad, or from public or private research centers.

L'archive ouverte pluridisciplinaire **HAL**, est destinée au dépôt et à la diffusion de documents scientifiques de niveau recherche, publiés ou non, émanant des établissements d'enseignement et de recherche français ou étrangers, des laboratoires publics ou privés.

Atomic-Spring Effect in Amorphous Silica-Helium Composites

Daniel T. Bowron¹, David A. Keen¹, Mathieu Kint², Coralie Weigel², Leszek Konczewicz^{2,3}, Sylvie Contreras², Benoit Coasne⁴, Gaston Garbarino⁵, Mickael Beaudhuin⁶, Julien Haines⁶, Jérôme Rouquette⁶

¹ *ISIS Facility, Rutherford Appleton Laboratory, Harwell Campus, Didcot, OX11 0QX, UK*

² *L2C, Univ Montpellier, CNRS, Montpellier, France*

³ *Institut of High Pressure Physics, Polish Academy of Sciences, Sokolowska 29/37, 01-142 Warsaw, Poland.*

⁴ *Univ. Grenoble Alpes, CNRS, LIPhy, 38000 Grenoble, France*

⁵ *ESRF, 38000 Grenoble, France*

⁶ *ICGM, Univ Montpellier, CNRS, ENSCM, Montpellier, France*

Abstract

Amorphous materials are structurally complex compounds, some of which exhibit network glass topologies, with on-going fundamental questions on their local^{1,2}/intermediate^{3,4} orders, transitions between ‘polyamorphs’^{5,6} or in the liquid state^{7,8}. These features, which are responsible for interesting physical properties, are widely used in optical and electronic devices as found in the special case of the archetype amorphous silica, α -silica. Here we determine the structural origin of an “atomic-spring effect” in an amorphous silica-helium composite, which exhibits a mechanical property that reversibly accumulates and restores energy at the subnanoscale. Such an “atomic-spring mechanical property” is shown to arise from the reversible elastic distortion of the glass network due to the presence of helium, mainly in six-membered rings of SiO₄ tetrahedra, under pressure. Based on an experimental pair distribution function study combined with atom-scale molecular simulations, the compression behaviour of the amorphous silica-helium composite is structurally characterized by the appearance of a uni-to-bi-modal distribution in the inter-tetrahedral distances in the amorphous isotropic structure of silica. We propose a simple characterization of this atomic-spring glass property using impedance spectroscopy measurements.

Finding new ways to accumulate and restore mechanical energy at the nanoscale is highly desirable, particularly when a solution is found for the archetype glassy material: amorphous silica SiO_2 , *a*-silica, which exhibits both fundamental and technological interest. An atomic-spring could be used in subnanoscale devices and sensors to measure “nano” forces and would offer an outstanding energy dissipation mechanism. The *a*-silica-He composite does not, at first instance, appear as an appropriate candidate for such an issue as *a*-silica is not defined as a porous material and only 0.0084 mol/cm³/GPa of He were found to be inserted in *a*-silica at pressures up to 0.13 GPa⁹. However, *a*- SiO_2 exhibits a corner-sharing SiO_4 tetrahedra local structure which forms voids of *n*-fold rings (with $n \geq 2$, in *a*- SiO_2 mostly $n = 4, 5, 6, 7, 8$)^{1,3,10-12}, the diameter of which is large enough for He ($r_{\text{He}}=1.3 \text{ \AA}$) to be inserted under pressure in the most common six-membered units¹³, ($r_{6\text{-fold ring}}=1.5 \text{ \AA}$). This scenario was confirmed and up to 1 mole of He could be inserted experimentally¹⁴⁻¹⁶ (0.53 mole theoretically)¹⁷ in *a*-silica under pressure. Interestingly, He as a pressurization fluid can be considered as a penetrating medium, whereas Ar atoms ($r_{\text{Ar}}=1.88 \text{ \AA}$), cannot be inserted so that pressurization using this fluid results in the normal densification of the material under compression. So far, the mechanism of helium insertion has never been determined, so to gain insight we performed an *in situ* structural investigation of helium insertion in *a*-silica at the beamline ID27 of the European Synchrotron Radiation Facility (ESRF) based on a high-pressure pair distribution function study (HP-PDF). High-quality PDFs require high-energy photons and access to large scattering angles to measure data to high values of momentum transfer ($Q = 4\pi \sin \theta/\lambda$)^{1,12,18}. In addition, in order to obtain reliable HP-PDF, Bragg and Compton scattering from the diamond anvils have to be removed. These surprising experimental results were made possible by using a large area detector and by subtracting the scattered intensity of the 3 μm -spot size-61 keV beam due to helium from the *a*-silica signal at the same focal point¹⁹ for each pressure point (Extended data, Fig. 1). The raw detector image data are shown in Extended data, Fig. 2, whilst reduced and corrected data at *Patm* and 8.8 GPa used for structural modelling are shown in Figure 1. The X-ray structure factor of *a*-silica obtained at *Patm* in the diamond cell up to $Q = 22.5 \text{ \AA}^{-1}$ along with the structure factor calculated from an empirical potential structure refinement (EPSR) model^{20,21} are shown on Figure 1. Upon increasing pressure, the first sharp peak of the X-ray structure factor of *a*-silica decreases in intensity and broadens up to the

highest pressure reached, Figure 1b (see also Extended Data Fig. 3). The comparison of the partial radial distribution functions obtained from the EPSR model with those simulated by molecular dynamics using the CHIK-potential²² show very good agreement and are shown in Extended Data Fig. 4. This consistency between the two modelling approaches enhances our confidence that the local structure of *a*-silica derived by our atomistic structure refinement of the experimental scattering data is robust. In the EPSR structural model, the helium inserted values N_{He}^P at each pressure point were fixed to those determined using a poromechanical model relying on atom-scale Grand Canonical Monte Carlo simulations¹⁷, see Extended data Fig. 5. The partial radial distribution functions for Si-Si, Si-O, O-He obtained from the EPSR model are shown on Figure 2a-c, respectively. These data provide a means of understanding the structural modifications induced by the helium insertion at high pressure. The pressure induced changes consist of: i) a broadening of the Si-Si distance distribution (inter-tetrahedral distances) between the first and second coordination shells (Figure 2a), which additionally results in the appearance of a new contribution, observed above 3 Å, in the Si-O RDF (Figure 2b), and ii) a decrease in the O-He distance distribution with increasing pressure, which becomes sharper as a result of helium confinement (Figure 2c). Based on the EPSR model, access to bond angle distributions was possible and the Si-O-Si distributions are shown in Fig. 2d. This representation gives the probability of a given bond angle, $P(\theta_{Si-O-Si})$, and is corrected for solid angle sampling, where the number of angles available at an angle θ is proportional to $\sin \theta$ ^{23,24}; the estimation of the mean bond angle values can be obtained as the sum of these probabilities $P(\theta_{Si-O-Si})$ is equal to 1, so the mean is simply the point where $\Sigma(P(\theta_{Si-O-Si}))$ is 50% (Extended data Fig. 6). At *Patm* the Si-O-Si angle was found to have a mean value of 164° that is in agreement with literature reports from first principles calculations^{25,26}, PDF^{18,27} and NMR studies²⁸. As already observed in Figure 2a with the Si-Si distance distribution, increasing pressure results in a change from a uni- to a bi-modal Si-O-Si bond angle distribution with the mean value decreasing from 164° to 161° at the highest pressure reached.

In order to understand the change in the local structure of *a*-silica due to helium insertion characterized by HP-PDF, it is particularly interesting to note the structural consequences of compression/gas insertion in microporous silica. In siliceous zeolites, compression behaviour is generally associated with changes in inter-tetrahedral bridging angles in the SiO₂ framework resulting in a strong increase in pore ellipticity²⁹; such a mechanism can be blocked by gas insertion, which will fill pores and prevent pore collapse³⁰⁻³². As previously mentioned, the local structure of *a*-silica is defined by corner-sharing SiO₄ tetrahedra forming *n*-fold rings. During He-insertion, He-atoms ($r_{He}=1.3$ Å) are small

enough: i) to be inserted under pressure in the most common six-membered rings¹³ ($r_{6\text{-fold ring}} = 1.5 \text{ \AA}$) and prevent collapse of the framework and ii) to induce a change from uni- to bi-modal distribution in the inter-tetrahedra distance, which could be considered as a local distortion of the ring as determined by this HP-PDF study. Compression behaviour of *a*-silica in He therefore induces a splitting in the Si-Si distance distribution (Fig.2a) associated with the appearance of a new contribution in the Si-O pair correlations at approximately 3 Å (Fig.2b) and induces a bimodal Si-O-Si bond angle distribution (Fig. 2d). Figure 3a schematically represents the mechanism of He-insertion in a six-membered rings, in which insertion of He-atoms acts as an atomic-spring preventing ring collapse and inducing a local distortion under compression. Note that the He-insertion induced appearance of a local distortion could not be predicted in the poromechanical model as such a microscopic change in the local structure would require density functional theory calculations using a similar *a*-silica cell dimension as those of the models used here, which is not currently achievable⁶.

In order to characterize He-insertion in *a*-silica, which is found to exhibit an atomic-spring effect as described above, Sato et al. previously reported microscopic observation of the system to estimate the equation of state of *a*-silica in a penetrating (He) and non-penetrating medium (methanol-ethanol)¹⁴. Later, Weigel et al.³³ used the Clausius-Mossotti relationship to estimate the helium inserted values N_{He}^P based on the measurement of the refractive index in *a*-silica, studied by Brillouin spectroscopy³⁴. Due to the relationship between refractive index, dielectric permittivity and complex impedance, spring glass properties of the *a*-silica-He composite can then be determined by impedance spectroscopy (Extended data Fig. 7). Figure 3b shows the pressure dependence of the relative impedance data (Z/Z_0) obtained for *a*-silica in a penetrating (He), i.e. atomic-spring, and non-penetrating medium (gasoline F) up to 1.6 GPa during compression/decompression. It is interesting to note first that both data exhibit an equation of state-like profile with Z/Z_0 values higher in He than those in gasoline. Data are perfectly reproducible under decompression and this is consistent with a reversible mechanism of He insertion/ removal along with the atomic-spring effect. Additionally, relative impedance values for a penetrating/non penetrating medium at the highest pressure reached, i.e. $\sim 0.957/0.932$, are in qualitative agreement with those reported for V/V_0 ($\sim 0.975/0.95$); notably, the impedance difference value is similar to that of the volume difference between the two sets of data in a penetrating/non penetrating medium ($\sim 2.5\%$). Impedance spectroscopy measurements probe an absence of change in the electron density of state in *a*-silica within this pressure-range, which depends therefore only on the volume; this is why one can understand such similarities between Z/Z_0 and

V/V_0 data. Note that estimated values of the relative volume based on impedance measurement are probably more accurate than those estimated by microscopic observation due to a greater sensitivity and resolution.

The present study has allowed us to determine the structural mechanism linked to He-insertion in α -silica based on an EPSR model, which was only possible due to the ability of obtaining accurate X-ray structure factors up to $Q = 22.5 \text{ \AA}^{-1}$. As previously mentioned, from a poromechanical perspective, up to 0.5 mole of He can be inserted in the most common six-membered rings, both preventing the collapse of the ring due to atomic-spring effect and inducing a local distortion in the isotropic glass matrix. Such a composite can easily be achieved and characterized as shown by the present example of impedance spectroscopy measurements.

We expect that the present finding will stimulate further investigation in order to use such an effect in applications in subnanoscale devices and sensors.

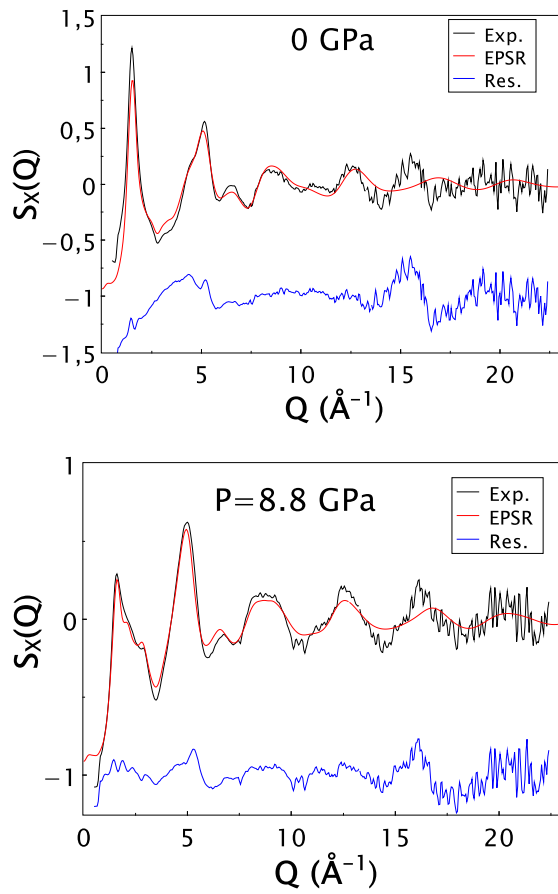


Fig. 1 | *a*-silica-He composite structure factor $S_x(Q)$ (black). **a**, at *Patm*, **b**, at 8.8 GPa; red and blue lines show calculated EPSR model and the difference between calculated and experimental data, respectively.

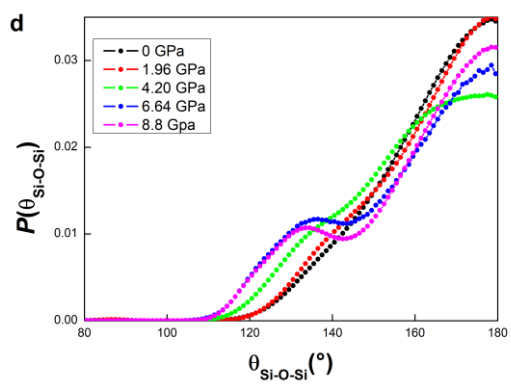
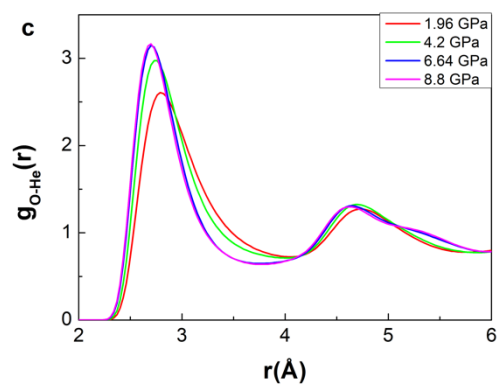
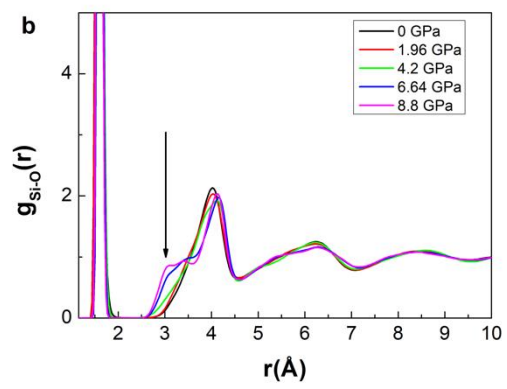
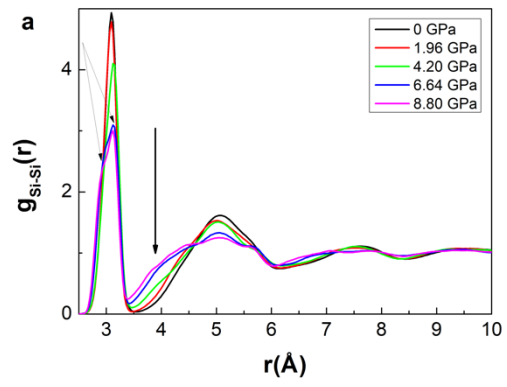


Fig. 2 | Pressure dependence of the partial radial distribution functions from EPSR model of *a*-silica-He composite. **a, $g_{Si-Si}(r)$, **b**, $g_{Si-Si}(r)$, **c**, $g_{O-He}(r)$; arrows either show the appearance of a bi-modal distribution or of a new contribution, and **d**, Pressure dependence of Si-O-Si bond angle distribution functions.**

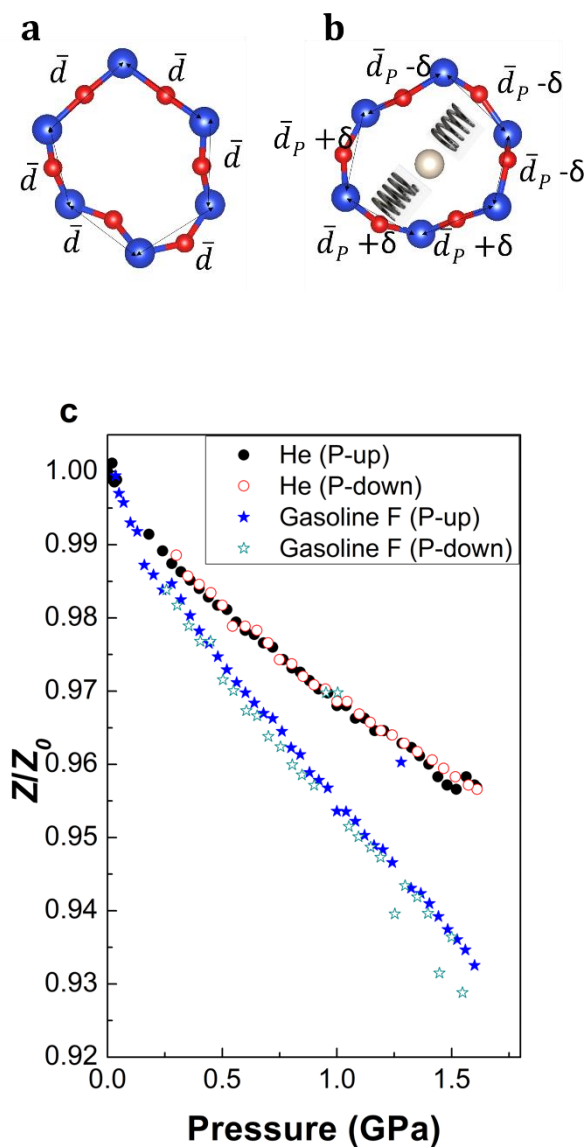


Fig. 3 | Atomic-spring effect in *a*-silica. Mechanism of He-insertion in an example of a six-membered rings obtained **a**, at P_{atm} and at **b**, 8.8 GPa from PDF data, in which the presence of He-atoms acts as an atomic-spring preventing ring collapse and inducing uninomodal (\bar{d})-to-bimodal ($\bar{d}_P + \delta$, $\bar{d}_P - \delta$) distribution of the inter-tetrahedral distance; red, blue and white spheres represent Si and O and He atoms respectively **c**, Pressure dependence of the relative impedance measurements (obtained at 2 MHz) on a penetrating medium (He) and on a non-penetrating medium (Gasoline F)

Methods

High-Pressure Pair Distribution Function Study

The *a*-silica sample consists of a 54 μm thick Suprasil F300 platelet containing less than 1ppm OH (Heraeus Quartzglass, Germany), which was measured as a function of pressure up to 8.8 GPa using a diamond anvil cell at room temperature using helium as pressure transmitting medium and ruby sphere to measure pressure calibration (ref), Extended data Fig. 1.

X-ray energy of 61keV and a Perkin-Elmer flat panel large area detector was used on ID27 at the ESRF.

Accurate structure factors of the *a*-silica-He composite were obtained by subtracting the intensity of the 3 μm -spot size-61 KeV beam from air/Helium to the *a*-silica signal at the same focal points for each pressure data allowing reliable diffraction patterns to be obtained up to a maximum scattering of $Q \sim 23 \text{ \AA}^{-1}$, Extended data Fig . 2.

Empirical Potential Structure Refinement (EPSR)

EPSR uses a simple Lennard-Jones + Coulomb pair-wise potential to restrain the model, as well as the data. The L-J parameters were chosen to mimic the Van der Waals radii and were fixed at the same value for all pressures. The coulomb charges were +2 (Si), -1 (O) and 0 (He).

The comparison of the obtained partial radial distribution functions obtained from the EPSR model with those simulated by molecular dynamics using the CHIK-potential¹ show a perfect agreement, Extended data Fig. 3, which definitely validates our strategy to characterize the local structure of *a*-silica.

In the EPSR structural model, the helium inserted values N_{He}^P at each pressure points were fixed to those determined using a poromechanical model¹⁸, Extended data Fig . 4.

High-Pressure Impedance Spectroscopy Study

The Clausius-Mossotti relationship for *a*-silica-He composite can be written as:

$$3\varepsilon_0 \frac{n^2 - 1}{n^2 + 2} = N_{\text{SiO}_2} \alpha_{\text{SiO}_2} + N_{\text{He}} \alpha_{\text{He}}$$

ε_0 : permittivity of free space

$n = n_{a\text{-SiO}_2}^{\text{He}}$: refractive index of the composite

N_{SiO_2} , N_{He} : density values of SiO₂ and He

α_{SiO_2} , α_{He} : polarizability of SiO₂ and He

Impedance measurements as a function of frequency 100 kHz–3 MHz were performed up to 1.6 GPa on *a*-silica (Suprasil F300) disk of (dimensions) metallized with gold on both faces, Extended data Fig. 7, with a Rhode Schwartz impedance analyzer on the third stage of a Unipress gas compressor using either a penetrating (He), i.e. atomic-spring, and a non- penetrating medium (gasoline F). The pressure was measured with a manganin gauge.

Acknowledgements

The authors thank Olivier Cambon for his help on impedance measurements as well as Patrick Hermet for data extraction, Benoit Rufflé and Marie Forêt for stimulating discussions, the beamline ID27 from the ESRF.

Author contributions

Additional information

Supplementary information is available in the online version of the paper.

Correspondence and requests for materials should be addressed to.

References

- 1 Keen, D. A. & Dove, M. T. Local structures of amorphous and crystalline phases of silica, SiO₂, by neutron total scattering. *J. Phys.-Condes. Matter* **11**, 9263-9273, doi:10.1088/0953-8984/11/47/311 (1999).
- 2 Sheng, H. W., Luo, W. K., Alamgir, F. M., Bai, J. M. & Ma, E. Atomic packing and short-to-medium-range order in metallic glasses. *Nature* **439**, 419-425, doi:10.1038/nature04421 (2006).
- 3 Elliott, S. R. Medium-range structural order in covalent amorphous solids. *Nature* **354**, 445-452, doi:10.1038/354445a0 (1991).
- 4 Keen, D. A. & Goodwin, A. L. The crystallography of correlated disorder. *Nature* **521**, 303-309, doi:10.1038/nature14453 (2015).
- 5 Wilding, M. C., Wilson, M. & McMillan, P. F. Structural studies and polymorphism in amorphous solids and liquids at high pressure. *Chem. Soc. Rev.* **35**, 964-986, doi:10.1039/b517775h (2006).
- 6 Deringer, V. L. *et al.* Origins of structural and electronic transitions in disordered silicon. *Nature* **589**, 59-64, doi:10.1038/s41586-020-03072-z (2021).
- 7 Debenedetti, P. G., Sciortino, F. & Zerze, G. H. Second critical point in two realistic models of water. *Science* **369**, 289-+, doi:10.1126/science.abb9796 (2020).
- 8 Henry, L. *et al.* Liquid-liquid transition and critical point in sulfur. *Nature* **584**, 382-+, doi:10.1038/s41586-020-2593-1 (2020).
- 9 Shelby, J. E. Pressure-dependence of helium and neon solubility in vitreous silica. *J. Appl. Phys.* **47**, 135-139, doi:10.1063/1.322359 (1976).
- 10 King, S. V. Ring configurations in a random network model of vitreous silica. *Nature* **213**, 1112-&, doi:10.1038/2131112a0 (1967).
- 11 Sarnthein, J., Pasquarello, A. & Car, R. Structural and electronic-properties of liquid and amorphous SiO₂ - An ab-initio molecular-dynamics study. *Phys. Rev. Lett.* **74**, 4682-4685, doi:10.1103/PhysRevLett.74.4682 (1995).
- 12 Tucker, M. G., Dove, M. T. & Keen, D. A. Application of the reverse Monte Carlo method to crystalline materials. *J. Appl. Crystallogr.* **34**, 630-638, doi:10.1107/s002188980100930x (2001).
- 13 Pasquarello, A. & Car, R. Identification of Raman defect lines as signatures of ring structures in vitreous silica. *Phys. Rev. Lett.* **80**, 5145-5147, doi:10.1103/PhysRevLett.80.5145 (1998).
- 14 Sato, T., Funamori, N. & Yagi, T. Helium penetrates into silica glass and reduces its compressibility. *Nat. Commun.* **2**, doi:10.1038/ncomms1343 (2011).
- 15 Shen, G. Y. *et al.* Effect of helium on structure and compression behavior of SiO₂ glass. *P Natl Acad Sci USA* **108**, 6004-6007, doi:10.1073/pnas.1102361108 (2011).

- 16 Weigel, C. *et al.* Vitreous Silica Distends in Helium Gas: Acoustic Versus Static Compressibilities. *Phys. Rev. Lett.* **109**, doi:10.1103/PhysRevLett.109.245504 (2012).
- 17 Coasne, B. *et al.* Poroelastic Theory Applied to the Adsorption-Induced Deformation of Vitreous Silica. *J Phys Chem B* **118**, 14519-14525, doi:10.1021/jp5094383 (2014).
- 18 Tucker, M. G., Keen, D. A., Dove, M. T. & Trachenko, K. Refinement of the Si-O-Si bond angle distribution in vitreous silica. *J. Phys.-Condes. Matter* **17**, S67-S75, doi:10.1088/0953-8984/17/5/008 (2005).
- 19 details are shown in SI
- 20 Soper, A. K. Partial structure factors from disordered materials diffraction data: An approach using empirical potential structure refinement. *Phys. Rev. B* **72**, doi:10.1103/PhysRevB.72.104204 (2005).
- 21 Bowron, D. T. An experimentally consistent atomistic structural model of silica glass. *Mater. Sci. Eng. B-Adv. Funct. Solid-State Mater.* **149**, 166-170, doi:10.1016/j.mseb.2007.11.030 (2008).
- 22 Carre, A., Horbach, J., Ispas, S. & Kob, W. New fitting scheme to obtain effective potential from Car-Parrinello molecular-dynamics simulations: Application to silica. *Epl* **82**, doi:10.1209/0295-5075/82/17001 (2008).
- 23 Kroon, J. & Kanters, J. A. Non-linearity of hydrogen bonds in molecular crystals. *Nature* **248**, 667-669, doi:10.1038/248667a0 (1974).
- 24 Baur, W. H. Straight si-o-si bridging bonds do exist in silicates and silicon dioxide polymorphs. *Acta Crystallogr. Sect. B-Struct. Sci. Cryst. Eng. Mat.* **36**, 2198-2202, doi:10.1107/s0567740880008382 (1980).
- 25 Umari, P., Gonze, X. & Pasquarello, A. Concentration of Small Ring Structures in Vitreous Silica from a First-Principles Analysis of the Raman Spectrum. *Phys. Rev. Lett.* **90**, 027401, doi:10.1103/PhysRevLett.90.027401 (2003).
- 26 Giacomazzi, L., Umari, P. & Pasquarello, A. Medium-range structure of vitreous SiO_2 obtained through first-principles investigation of vibrational spectra. *Phys. Rev. B* **79**, 064202, doi:10.1103/PhysRevB.79.064202 (2009).
- 27 Kohara, S. & Suzuya, K. Intermediate-range order in vitreous SiO_2 and GeO_2 . *Journal of Physics: Condensed Matter* **17**, S77-S86, doi:10.1088/0953-8984/17/5/009 (2005).
- 28 Mauri, F., Pasquarello, A., Pfrommer, B. G., Yoon, Y.-G. & Louie, S. G. Si-O-Si bond-angle distribution in vitreous silica from first-principles ^{29}Si NMR analysis. *Phys. Rev. B* **62**, R4786-R4789, doi:10.1103/PhysRevB.62.R4786 (2000).

- 29 Thibaud, J. M. *et al.* High-Pressure Phase Transition, Pore Collapse, and Amorphization in the Siliceous 1D Zeolite, TON. *J. Phys. Chem. C* **121**, 4283-4292, doi:10.1021/acs.jpcc.6b11594 (2017).
- 30 Colligan, M. *et al.* Synchrotron X-ray powder diffraction and computational investigation of purely siliceous zeolite Y under pressure. *J. Am. Chem. Soc.* **126**, 12015-12022, doi:10.1021/ja048685g (2004).
- 31 Arletti, R. *et al.* Pressure-induced penetration of guest molecules in high-silica zeolites: the case of mordenite. *Phys Chem Chem Phys* **17**, 24262-24274, doi:10.1039/c5cp03561a (2015).
- 32 Thibaud, J. M. *et al.* Saturation, of the Siliceous Zeolite TON with Neon at High Pressure. *J. Phys. Chem. C* **122**, 8455-8460, doi:10.1021/acs.jpcc.8b01827 (2018).
- 33 Weigel, C. *et al.* Vitreous Silica Distends in Helium Gas: Acoustic Versus Static Compressibilities. *Phys. Rev. Lett.* **109**, 245504, doi:10.1103/PhysRevLett.109.245504 (2012).